Journal of Fluids and Structures (2002) **16**(4), 453–463
doi:10.1006/jfls.2001.0431, available online at http://www.idealibrary.com on IDEAL®

OBLIQUE VORTEX SHEDDING BEHIND TAPERED CYLINDERS†

B. VALLÈS AND H. I. ANDERSSON

Department of Applied Mechanics, Thermodynamics and Fluid Dynamics
Norwegian University of Science and Technology, N-7491 Trondheim, Norway

AND

C. B. JENSSEN

Statoil R&D Centre, N-7005 Trondheim, Norway

(Received 22 November 2000, and in final form 20 September 2001)

The vortex shedding in the wake behind linearly tapered circular cylinders has been considered for the two taper ratios 75:1 and 100:1. The Reynolds number based on the velocity of the incoming flow and the largest diameter was in the range from 130 to 180. The low Reynolds number assured that laminar flow prevailed in the entire flow field. The full unsteady three-dimensional Navier–Stokes equations were solved numerically with the view of exploring the rather complex vortex shedding phenomena caused by the variation of the natural shedding frequency along the span of the cylinder. The accurate computer simulations showed that this variation gave rise to discrete shedding cells, each with its own characteristic frequency and inclined with respect to the axis of the cylinder. Flow visualizations revealed that vortex dislocation and splitting took place in the numerically simulated flow fields. The computer simulations compared surprisingly well with the extensive laboratory experiments reported by Piccirillo & Van Atta in 1993 for a range of comparable conditions; this has enabled detailed analyses of other flow variables (notably pressure and vorticity) than those readily accessible in a physical experiment. However, distinct differences in the vortex dynamics are observed in some of the cases.

1. INTRODUCTION

THE POTENTIALLY SEVERE CONSEQUENCES of vortex shedding behind bluff bodies was a completely unknown phenomenon among most civil engineers until the collapse of Tacoma bridge some 50 years ago. Today, the vortex dynamics in wakes behind geometrically simple objects are quite well understood as long as the shedding is nominally two-dimensional (2-D); see the excellent review by Williamson (1996). Three-dimensional (3-D) vortex shedding is by far more complex from a physical point of view and therefore relatively less well understood. 3-D wake phenomena may for example occur behind circular cylinders if U/D varies along the span of the cylinder, i.e., if either (or both) the cylinder diameter D or the incoming velocity U changes. A geometrically simple configuration, and yet one of great practical relevance (e.g., chimneys and oil-platform legs), is the uniform flow past a linearly tapered circular cylinder, of which a slender cone represents a special case. Following the pioneering experimental studies by Gaster (1969, 1971), in-depth laboratory investigations

†This paper is based on an oral presentation at the IUTAM Symposium on Bluff Body Wakes and Vortex-Induced Vibrations held in Carry-le-Rouet outside Marseille, France 13–16 June, 2000.

0889–9746/02/040453 + 13 $35.00/0

of vortex shedding behind tapered cylinders were performed by Piccirillo & Van Atta (1993), and Papangelou (1992) for the special case of cones, and more recently by Hsiao & Chiang (1998).

Until recently, the majority of investigations of 3-D vortex shedding were performed in the laboratory. Computer simulations, which require accurate solutions of the time-dependent 3-D Navier–Stokes equations, have only become feasible in the last decade, e.g., Jespersen & Levit (1991). The objective of the present study is to perform detailed computer simulations of the 3-D laminar vortex shedding behind a linearly tapered cylinder with a two-fold aim: (i) to demonstrate how closely the experimental findings of Piccirillo & Van Atta (1993) can be reproduced numerically; and (ii) to explore the simulated flow fields with the view to provide details of the complex shedding pattern not readily available in a laboratory experiment. First, however, a brief summary of the most striking vortex shedding phenomena is provided.

2. VORTEX SHEDDING PHENOMENA

The vortex shedding behind a straight circular cylinder in a uniform incoming flow is a classical example of naturally occurring unsteadiness in fluid dynamics. Following Roshko in 1954, numerous authors have contributed experimentally, theoretically and numerically to the understanding of intricate and fascinating phenomena such as vortex shedding, vortex splitting, oblique versus parallel shedding, and the occurrence of flow instabilities (Modes A and B) in the transition-to-turbulence process; see Williamson (1996) for details. For example, a subject of controversy has been the origin of discontinuities in the Strouhal–Reynolds number relationship in the laminar shedding regime (Gaster 1969, 1971; and Tritton 1959, 1971). Williamson (1988) showed that in the parallel shedding regime, the Strouhal–Reynolds number curve was completely continuous. Moreover, the experimental oblique-shedding data closely collapsed onto the parallel-shedding curve, defining a universal Strouhal–Reynolds number curve:

$$\mathrm{St} = \frac{A}{\mathrm{Re}} + B + C\,\mathrm{Re}, \tag{1}$$

where $A = -3{\cdot}3265$, $B = 0{\cdot}1816$ and $C = 1{\cdot}600 \times 10^{-4}$, and the Reynolds number is defined as $\mathrm{Re} = UD/\nu$, with ν the kinematic viscosity of the fluid. Similarly the Strouhal number, which is a dimensionless frequency parameter, can be defined as $\mathrm{St} = fD/U$, where f denotes the vortex shedding frequency. Williamson & Brown (1998) showed that a more accurate St–Re relationship could be given by

$$\mathrm{St} = A + \frac{B}{\sqrt{\mathrm{Re}}} + \frac{C}{\mathrm{Re}}, \tag{2}$$

where $A = 0{\cdot}2850$, $B = -1{\cdot}3897$ and $C = 1{\cdot}8061$. According to Williamson & Brown (1998), equation (2) with this set of coefficients is "distinctly more accurate than existing traditional fits".

Next, in order to investigate a somewhat more complex problem, two variants can be studied: a change in incoming flow (even if the uniformity assumption can often be made, in reality this never happens), or a change in geometry (for industrial applications). The former configuration consists of an incoming linear shear flow past a uniform circular cylinder; the linear shear flow means that the velocity u of the incoming stream varies linearly along the z-axis which is the cylinder axis [see Figure 1(a)]. The latter case is that of a uniform incoming flow (U) past a tapered circular cylinder; the taper implies a constant change in

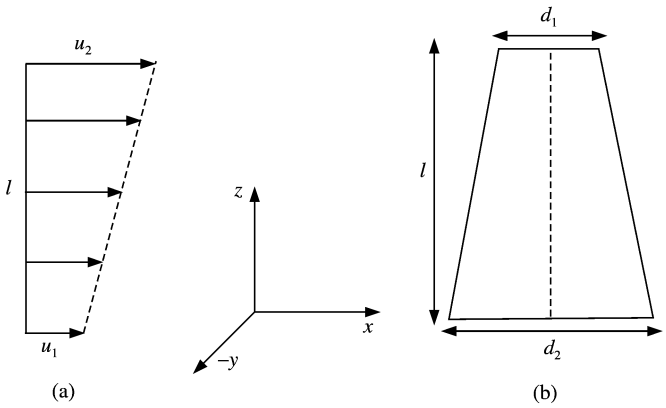

Figure 1. Sketch of: (a) linear shear flow, (b) tapered cylinder.

diameter d all along the span [see Figure 1(b)]. The former is characterized by a shear parameter: $\beta = (D/u_m)(\partial u/\partial z)$, where D is the diameter of the circular cylinder and u_m denotes the average free-stream velocity. The latter is characterized by the taper ratio: $R_T = l/(d_2 - d_1)$, where l is the length of the cylinder, and d_2 and d_1 denote the diameters of the wide and narrow ends of the cylinder, respectively. The two flow configurations depicted in Figure (1) may at first sight appear fundamentally different. However, the observed vortex shedding phenomena turn out to be quite similar [see the review on vortex shedding from bluff bodies in shear flow by Griffin (1985)]. Indeed, by assuming that the same fluid is considered in both cases and that $u_m = U$, the relation $\beta = 1/R_T$ is easily obtained, thereby justifying at least qualitative comparisons. This suggests the alternative definition $(d_2 - d_1)/l$ for the taper ratio.

Nevertheless, an important distinction between the linear shear flow and the uniform flow past a tapered cylinder should be pointed out. In the former case, the local stagnation pressure varies essentially proportionally to u^2, as does the base pressure along the lee side; see, e.g., Zdravkovich (1997). The associated pressure gradients along the span give rise to a pressure-driven secondary flow along the stagnation line from the high-velocity end towards the low-velocity end, and an oppositely directed flow along the lee side of the cylinder. In the tapered case, on the other hand, the stagnation pressure and the base pressure are practically constant along the span and no such secondary motions are set up.

Another particularly attractive feature of the flow over a tapered cylinder is that end effects can be completely eliminated by proper choice of boundary conditions in the spanwise direction. This contrasts with the linear shear flow case, in which the influence of end conditions cannot be avoided (Mukhopadhyay *et al.* 1999), as shown in the investigation of end effects by Mair & Stansby (1975). This motivates the present computer experiments on flow phenomena in the wake behind a tapered straight circular cylinder in an originally uniform stream.

Three main features of the vortex dynamics in tapered cylinder wakes should be noted: the characteristic cell pattern, the oblique shedding angle, and vortex dislocation (Williamson 1989) or vortex splitting (Eisenlohr & Eckelmann 1989). Since the earliest work of Gaster (1969), the vortex-cell shedding has been proved to be an important characteristic of the vortex dynamics in the wake of a tapered cylinder (Noack *et al.* 1991) and sometimes also of the wake behind a nontapered straight cylinder (Williamson 1996). Piccirillo & Van Atta (1993) showed that the tapered cylinder span could be divided into a certain number of cells. Each cell was characterized by its own constant vortex shedding frequency. This

means that two neighbouring cells have shedding frequencies different from each other. Moreover, the size of the cells could be determined by the variation of the vortex shedding frequency along the spanwise direction: a sudden change in frequency indicated a change of cell.

After many years of controversy, it was pointed out by Williamson (1989) that the oblique shedding behind nontapered straight circular cylinders was caused by end effects, i.e., by disturbances originating from one end being propagated along the span from one shed vortex to another. For the tapered cylinders, on the contrary, it has been found by Piccirillo & Van Atta (1993) that the vortex shedding pattern was practically unaffected by end conditions. Hence, it seems that the oblique vortex shedding phenomenon of the tapered cylinders has a pure geometric origin. Piccirillo & Van Atta (1993) noticed that the bending of the vortex lines and the vortex splitting phenomenon were linked. Vortex splitting is said to occur when vortex lines of one core split apart to merge into the offset cores of neighbouring vortices (Eisenlohr & Eckelmann 1989). The angle between the shed vortices and the cylinder axis was observed to increase from 5 to 25°, before vortex splitting occurred. During each split, the vortex lines far away continue to steepen (up to 50°). After the split, the vortex lines again become continuous and slightly inclined with respect to the cylinder axis. Piccirillo & Van Atta moreover noticed that this bending of the vortex lines around the vortex split leads to a decrease in the local frequency of vortex shedding.

3. COMPUTATIONAL APPROACH

Piccirillo & Van Atta (1993) considered laminar vortex shedding behind four different circular cylinders with different taper ratios. In this paper, computer simulations are reported for three different cases, namely their Run 14 with $R_T = 100{:}1$, called Case A, and their Runs 22 and 23 with $R_T = 75{:}1$, called Cases B and C, respectively, see Table 1 for further details.

Each tapered cylinder was embedded in a 3-D computational mesh with 256 000 points. Based on the results of previous 2-D simulations (Vallès *et al.* 2001), this mesh size was found to be the best compromise between cpu-time consumption, storage requirements and resolution. The mesh was divided into 28 blocks. The cross-sectional view in Figure 2 shows how: six fine blocks form a ring surrounding the cylinder with eight coarser blocks outside the first ring in the x–y plane (cylinder cross-section). Two subdivisions were made in the z-direction, i.e., along the cylinder axis.

The parallelized Navier–Stokes solver concurrent block Jacobi (CBJ) adopted here is a parallel implicit multiblock time-accurate Navier–Stokes solver, with a coarse-grid correction scheme (CGCS). The CBJ code has been extensively tested and used by Jenssen (1994) and Jenssen & Weinerfelt (1995, 1998) to compute both steady and unsteady flow

TABLE 1
Computer simulations

Case	R_T	l/d_2	d_1/d_2	d_m/d_2	Re_{d_2} †	Run
A	100:1	37·473	0·625	0·707	178	14
B	75:1	33·461	0·556	0·631	131	22
C	75:1	33·461	0·556	0·631	163	23

† $\mathrm{Re}_{d_2} = Ud_2/\nu$, i.e., Reynolds number based on the largest diameter.

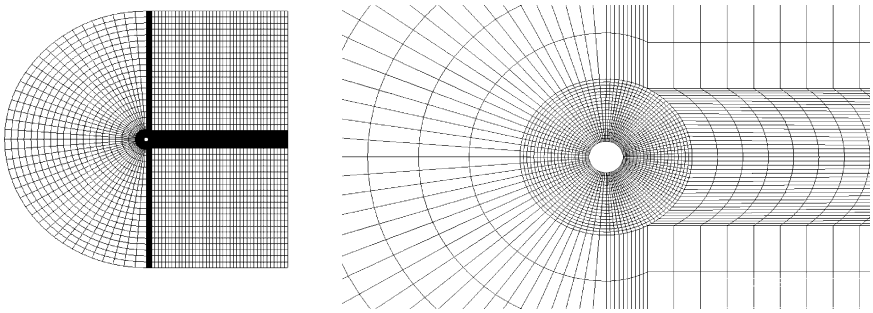

Figure 2. Three-dimensional mesh: view perpendicular to the axis of the cylinder. Left: complete view; right: close-up.

fields. The full time-dependent Navier–Stokes equations, written in integral form, were solved on the structured multiblock grid. The convective part of the fluxes was discretized with a third-order, upwind-biased method based on Roe's scheme. The viscous fluxes were obtained using central differencing. Derivatives of second-order accuracy are first calculated with respect to the grid indices and then transformed to derivatives with respect to the physical spatial coordinates. Implicit and second-order-accurate time-stepping was achieved by a three-point, A-stable, linear multistep method:

$$\frac{3}{2}(V_i/\Delta t)U_i^{n+1} - 2(V_i/\Delta t)U_i^n + \frac{1}{2}(V_i/\Delta t)U_i^{n-1} = R(U_i^{n+1}), \tag{3}$$

where the operator on the right-hand side denotes the sum of the flux into volume V_i of grid cell i, Δt is the time step, and n refers to the time level. To eliminate some of the end effects, Neumann-type boundary conditions were imposed on the $x - y$ planes at the two ends of the cylinder.

The computations were performed on a Cray T3E. The CBJ code ran on eight processors, each processor handled 32 000 points. The time step was fixed as $0{\cdot}1d_2/U$, or about $\frac{1}{50}$ of the shedding period. Each simulation was run for 500 time steps, i.e., roughly corresponding to ten shedding cycles. The dimensionless convergence criterion for the Newton iteration was 0·001 with a maximum of 20 Newton iterations per time step. The total consumption of cpu-time, after 500 time steps, was approximately 425 h, for both Cases A and B. This implies an average consumption of 6 cpu s per grid point, whereas the wall-clock time for each run was approximately 62 h. Thus, the use of eight processors in parallel on a Cray T3E enabled each simulation to be completed 7 times faster than on a computer with only a single processor.

4. RESULTS AND DISCUSSION

The cellular features of the vortex shedding can be visualized in different ways. Figure 3 gives the time evolution of the pressure field. The pressure values are taken on a line, parallel to the cylinder axis, at $x = 2{\cdot}5\,d_m$ and $y = 1\,d_m$, where d_m is the mean diameter given in Table 1. This detection line was offset $1d_m$ from the cylinder centre-line in order to detect only one side of the vortex street. The time-traces to the right in Figure 3 mimicked hot-wire outputs, and from these signals the vortex shedding frequencies at each spanwise location were calculated. By considering the variation in frequency between two neighbouring positions (cf. Section 2), in combination with both visualizations and animations of the flow, the number of shedding cells was determined for each of the three cases.

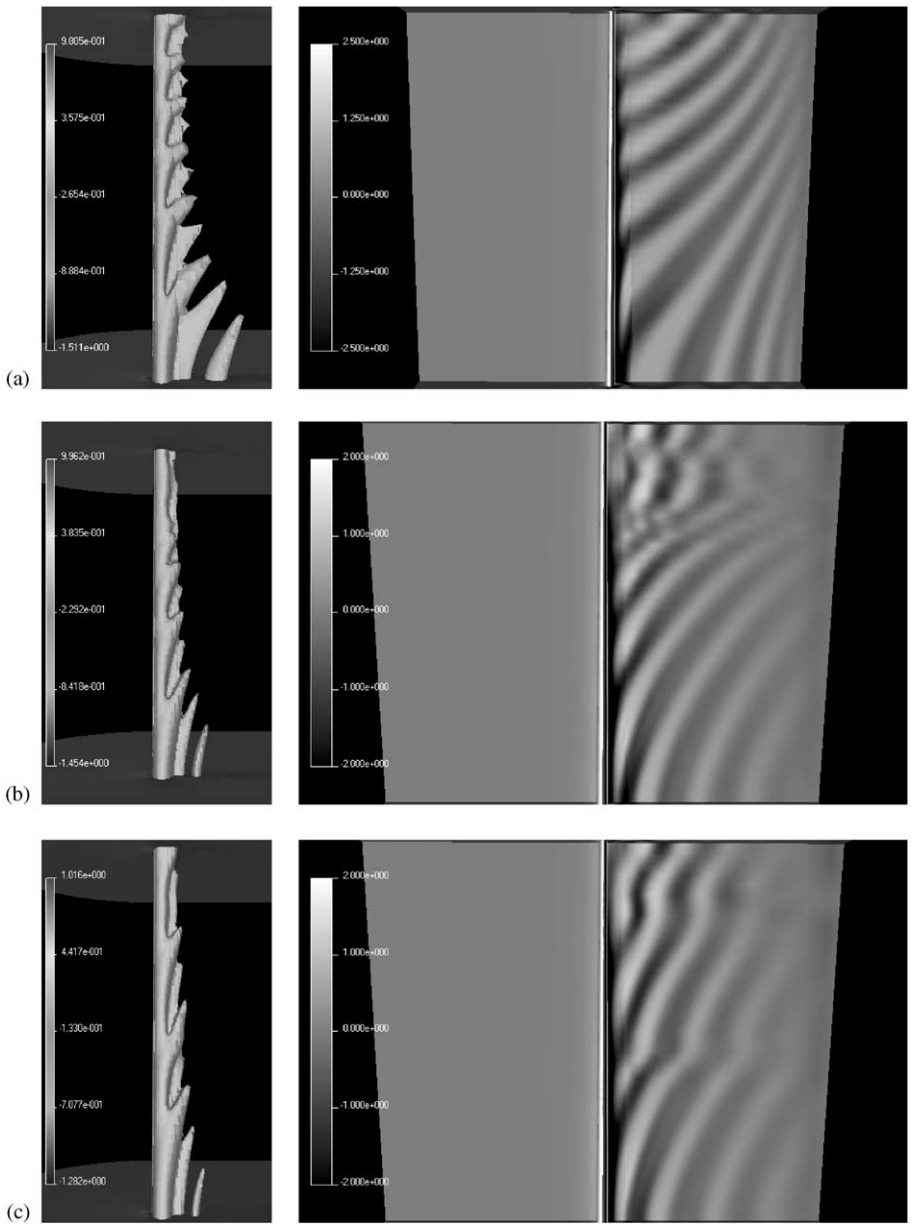

Figure 4. Instantaneous flow field: (a) Case A, (b) Case B and (c) Case C. At left, isopressure surface; at right, spanwise vorticity.

Instantaneous flow fields are shown in Figure 4. The characteristic cell pattern is clearly visible, both in the isosurfaces of pressure (to the left) and in the isocontours of the spanwise vorticity (to the right). When the end effects at the extremities of the cylinder are discarded, as in the study of Piccirillo & Van Atta (1993), four distinct shedding cells can be identified in Figure 4 for Case B, i.e., fully in accordance with the number of cells seen in the experiment. Although the positions of the cells were not completely fixed, the spanwise locations of the cell centres could be estimated on the basis of the computer simulations. These locations are shown versus local Strouhal number and local Reynolds number in

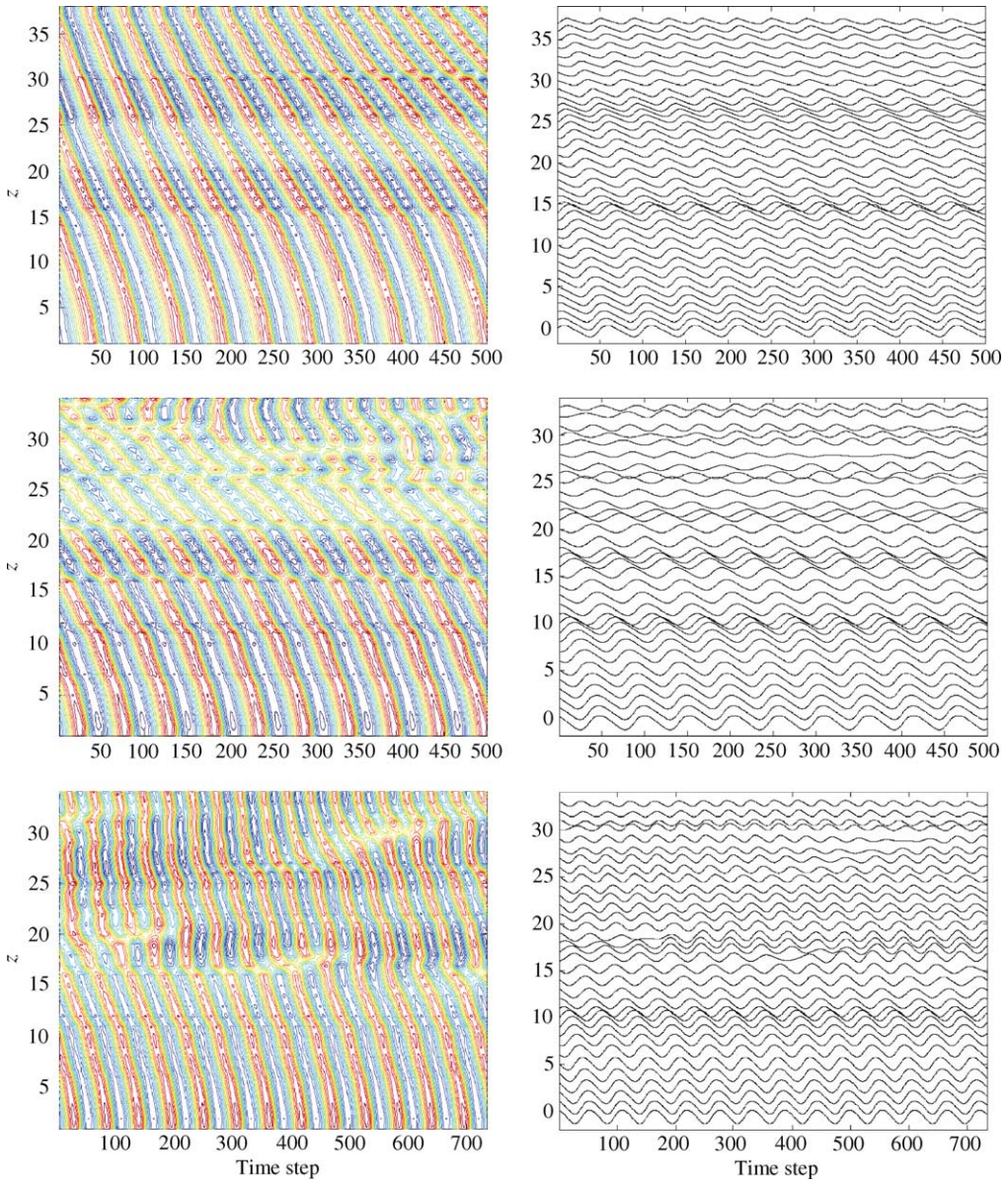

Figure 3. Time evolution of the pressure along the spanwise taken at $x = 2{\cdot}5d_m$ and $y = 1d_m$. From the top to the bottom: Case A, Case B and Case C. At left, isopressure contours; at right, pressure values at selected spanwise positions.

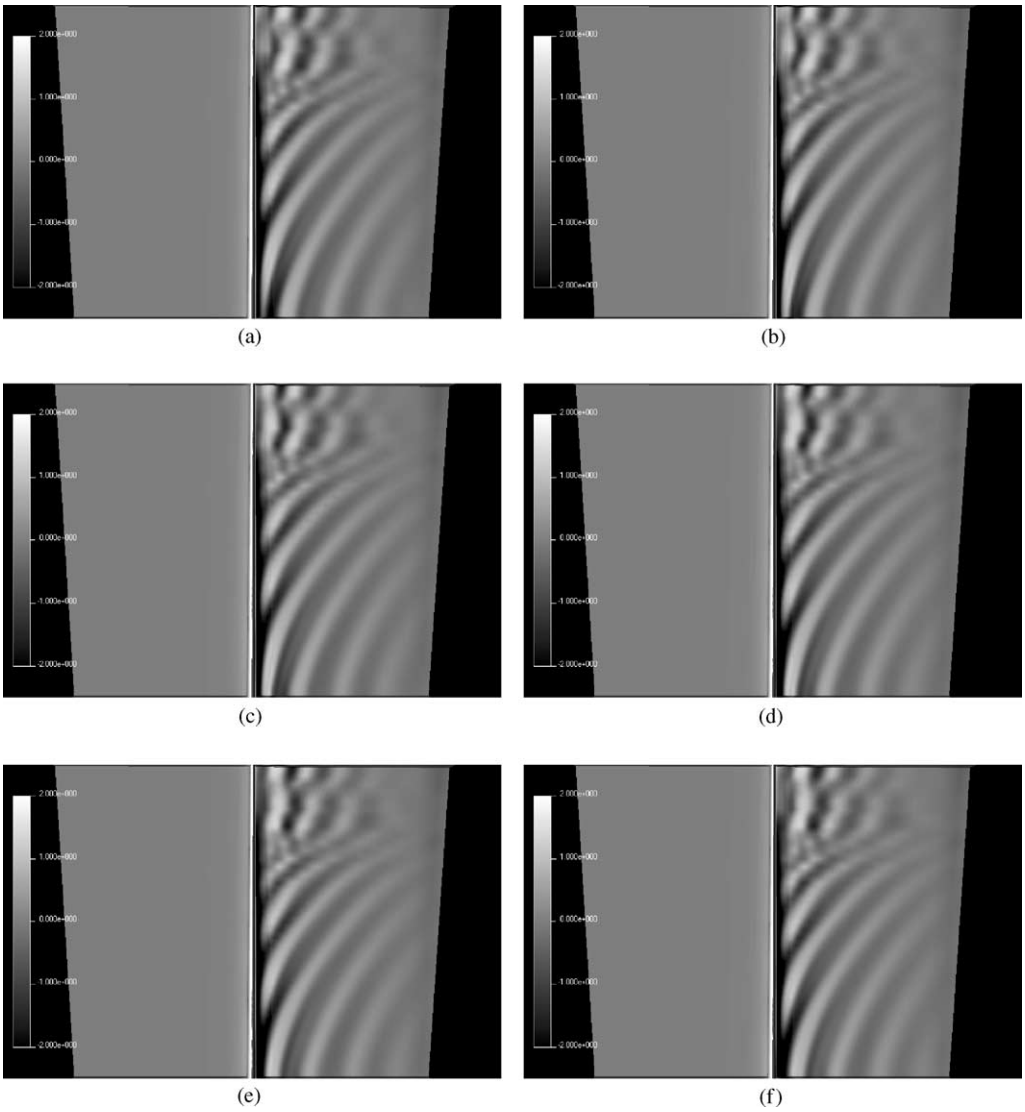

Figure 7. Time sequence of the instantaneous spanwise vorticity showing vortex splitting for Case B. Time steps: (a) 463, (b) 470, (c) 477, (d) 484, (e) 491, (f) 498.

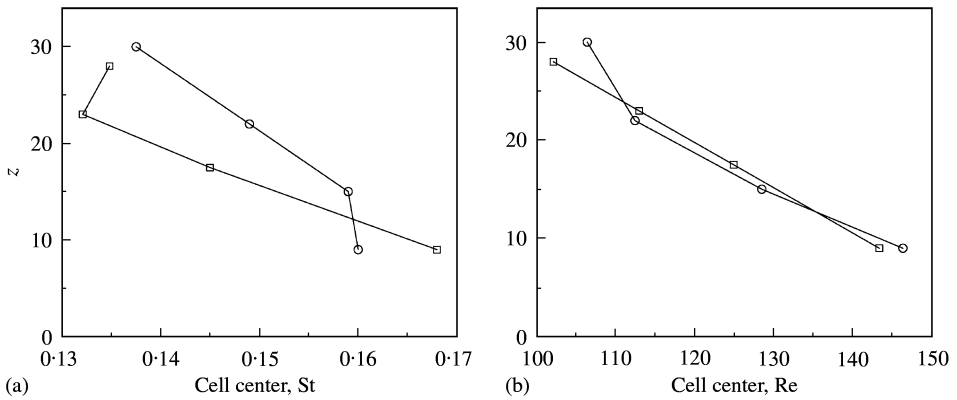

Figure 5. Cell mid-point locations for Case B (simulation), compared with experimental data from Piccirillo & Van Atta (1993) (experiment), plotted (a) versus local Strouhal number, (b) versus local Reynolds number: ○–○, experiment; □—□, simulation.

Figure 5 and compared with experimental data for Case B. The results of the computer experiments and the laboratory experiments show the same overall tendency, and the close correspondence between the local Reynolds numbers and the cell centre positions is particularly encouraging.

The situation is somewhat different for Case A, for which the time histories are shown at the top of Figure 3 and instantaneous flow fields in Figure 4. This flow field appears to be more regular than the two others (Cases B and C), with the cell positions being gradually shifted in the positive z direction, i.e., towards the narrow end of the cylinder. The same observation was made by Piccirillo & Van Atta (1993), namely that the flow field tends to be more chaotic with increased tapering (i.e., for lower taper ratios R_T). However, the isobars reveal the existence of five distinct cells, in accordance with the observed shift in the vortex shedding frequency, as deduced from the pressure time-histories. This latter finding is in conflict with the three shedding cells observed in the laboratory experiment. Analogous flow visualizations for Case C are shown at the bottom of Figures 3 and 4. Careful examination of the pressure contours to the left in Figure 3 suggests that a new cell is being created after about 200 time steps about midway between the cylinder ends. Similarly, a new cell is being formed after about 500 time steps. Altogether, four cells are visible at the same time. The experiments suggested that new cells were created near the wide end of the cylinder and gradually shifted towards the narrow end, just as in the present Case A. In Case C, however, the cells formed near the wide end of the cylinder are only shifted spanwise to about $z/d_2 = 15$.

A decade ago, Jespersen & Levit (1991) conducted similar 3-D simulations for laminar flow past a tapered cylinder with taper ratio $R_T = 100{:}1$ in a Reynolds number range from 90 to 145, i.e., somewhat lower than those considered in the present work. Their computations were performed on the massively parallel Connection machine with an implicit, approximate-factorization central-difference code for the full Navier–Stokes equations in generalized curvilinear coordinates and with a three-point implicit second-order time-stepping method.

Their results showed the same qualitative flow behaviour as the experiments of Piccirillo & Van Atta (1993) (i.e., velocity–time trace, vortex shedding), but some quantitative comparisons differed, such as the number of shedding vortex cells. An interesting result is that they got five cells, i.e., the same as in the present simulation.

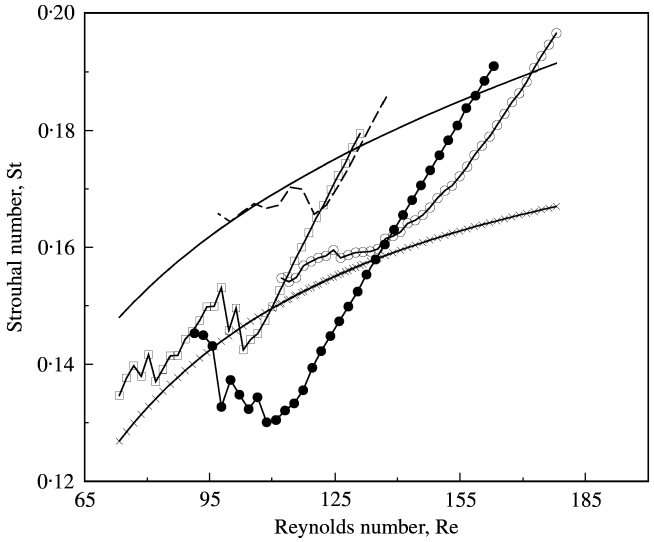

Figure 6. Local Strouhal number (St) versus local Reynolds number (Re). Cases A, B and C refer to the present simulations ○—○, Case A; ●—●, Case B; □—□, Case C; ▬, Williamson (1988); ×—×, Piccirillo & Van Atta (1993); – – –, Jespersen & Levit (1991). Jespersen & Levit's curve is for a simulation with $R_T = 100{:}1$. Piccirillo & Van Atta's curve is a fitting of all results reported by them. Williamson's curve is the universal St–Re curve in equation (1) for straight uniform circular cylinders.

The reason why both computer simulations were unable to reproduce the laboratory experiments in every detail is not clear. One explanation could be that the flow past a tapered circular cylinder with high taper ratio ($R_T = 100{:}1$) is more sensitive to end effects at the extremities of the cylinder than in cases with lower R_T. Indeed, tapered cylinders with taper ratios in the range considered here and by Jespersen & Levit (1991) are not very different from a uniform cylinder, the latter for which Williamson (1989) found that the end cells had a very strong effect on the main vortex shedding region. Moreover, Piccirillo & Van Atta (1993) noticed that: "For the 100:1 cylinder with $U = 0{\cdot}5$ cm/s the position of the cell boundaries changed by up to 1·0 cm, when nominally identical runs were compared." Consequently, we ought to state the same conclusion as them, namely that "care must be taken when using the cell boundary positions in quantitative analysis". The same behaviour was also described by Monkewitz (2000) during the recent IUTAM Symposium. It is noticeable that in the study of linear shear flow past straight uniform circular cylinders, essentially the same flow phenomena have been observed both experimentally by Mair & Stansby (1975), Stansby (1976) and Griffin (1985) and numerically by Mukhopadhyay *et al.* (1999).

In order to provide further qualitative comparisons, St(Re) curves were plotted in Figure 6. This figure compares the Strouhal–Reynolds relationships deduced from the present simulations with the results of the experiments by Piccirillo & Van Atta (1993). The curve-fit they employed was given by the relation $\mathrm{St}_c = 0{\cdot}195 - 5{\cdot}0/\mathrm{Re}$, where St_c is the Strouhal number associated with an individual shedding vortex cell. The St(Re) relations deduced from the simulations of Cases A and C are in good agreement with the experimental curve along one half of the cylinders (the narrowest part), i.e., for Re below 150 for Case A and below 115 for Case C, whereas the computations diverge from the experimental results for higher Reynolds numbers. This is mainly due to the fact that the experimental curve is a fit on Strouhal number values taken at the centre of each vortex cell only, whereas

the present results are based on a truly local Strouhal number for each spanwise location. The difference in spanwise boundary conditions in the experiment and the computations may also explain some of the deviations. A comparison between the simulation conducted by Jespersen & Levit (1991) with $R_T = 100{:}1$ and the present equivalent Case A in Figure 6, shows that the present results fit quite well with the experimental curve, while those of Jespersen & Levit (1991) are closer to the universal Strouhal–Reynolds number curve for uniform (i.e., nontapered) cylinders of Williamson (1988). This discrepancy is most likely due to the much coarser grid resolution used by Jespersen & Levit (1991). In conclusion, the present computer simulations showed that the local Strouhal number for tapered cylinders is lower than those for uniform cylinders at the same Reynolds number, fully consistent with earlier observations [Gaster 1969; Piccirillo & Van Atta 1993].

The St(Re) relation for Case B, however, seems to be in poor agreement with the experimental results. The only difference between the two simulations, Cases B and C, is the Reynolds number based on the wide diameter; cf. Table 1. This modest difference apparently affects the results considerably. By comparing the spanwise vorticity field in planes parallel to the axis of the cylinder in Figure 4 (c, right) and Figure 4 (b, right), a difference near the narrow (upper) end of the cylinder can be observed. In Case B a vortex splitting can be seen. In order to focus on this flow phenomenon, Figure 7 shows a time sequence of the vortex splitting. Considering positive spanwise vorticity (in white), a vortex shed approximately $l/3$ from the narrow end of the cylinder appears as three white spots in Figure 7(a). The split begins from the "second spot": a part of the main core of the vortex is merging into another vortex. Then, while the process evolves in time and space, carried away by the mean flow, the vortex lines surrounding the split seem to become more and more steep. In Figure 7(d), a second part of the main vortex splits to merge into the offset of a second vortex located behind the first one. Finally, in Figure 7(f) a new "main" vortex is shed from the same location as the first one.

This vortex splitting phenomenon explains what could be seen near the top of the pressure isocontours of Figure 3 (Case B). In the early stage of the process, four areas could be seen until the narrow-end cell began to grow from time step 250, thereby reducing the neighbouring shedding cell. Between time steps 250 and 300 only three cells could be seen. Then from time step 300 to 425, a change occurred and four areas could again be observed, probably due to a change of phase in the vortex shedding frequency. Finally, from time step 425 until the end of the process, the narrow-end cell considerably reduced its length and a new cell appeared with its centre approximately located at the interface between the previous cells.

Hence, the behaviour of the St(Re) relation in the Reynolds number range 95–125 for Case B, i.e., the decrease in local Strouhal number while the local Reynolds number is increasing, is believed to be due to the occurrence of the vortex splitting at the narrow end of the cylinder. In fact, the simulation showed exactly the same phenomena associated with the vortex splitting, as stated previously in Section 2, namely a decrease in the local vortex shedding frequency together with a bending of the vortex lines around the vortex split.

In the recent CFD analysis by Mukhopadhyay *et al.* (1999), most of the vortex shedding phenomena described above have been observed. Although they considered flow past a uniform cylinder, their linear variation of the incoming flow u caused a spanwise variation of u/D analogous to that in the present study. Their shear parameter β was equal to 0·02, and according to the relation in Section 2 this corresponds to uniform flow past a tapered cylinder with $R_T = 50{:}1$. Because this taper ratio is quite different from those in the present study, no qualitative comparisons have been made. Nevertheless, their numerical results compared well with experiments by Piccirillo & Van Atta (1993) for a tapered cylinder with $R_T = 50{:}1$.

5. CONCLUDING REMARKS

Accurate numerical solutions of the full time-dependent Navier–Stokes equations have been performed in order to provide an in-depth exploration of the intricate vortex shedding pattern in the wake of linearly tapered circular cylinders. The results for Cases A and C showed an encouraging consistency with the observations made by Piccirillo & Van Atta (1993). In particular, several important features of the oblique vortex shedding observed experimentally were reproduced by the computer simulations. These include the spanwise variation of the shedding frequency, which gives rise to discrete shedding cells, each with its own shedding frequency. For the tapered cylinder with $R_T = 75{:}1$, the number of vortex cells, as well as their inclination with respect to the axis of the cylinder, compared well with the experiment. The instantaneous vorticity fields mirrored the oblique vortex shedding pattern, whereas the isopressure contours showed that four distinct vortex cells were shed from the cylinder. Animations moreover revealed that the vortex shedding shifts along the span of the cylinder, from the narrow to the wide end. The vortex splitting phenomenon described by Piccirillo & Van Atta (1993) was observed to occur in the wake of the tapered cylinder in Case B.

It is noteworthy that the match with the experiments is not uniformly good. For instance, the variation of the Strouhal number along the span matches the experiments only in some of the cases. In other cases, the physics of the computed flow field is simply different from that of the laboratory flow, and distinct differences in the vortex dynamics are observed for the less tapered cylinders. Finally, striking similarities between uniform flow past tapered cylinders and linear shear flow past uniform circular cylinders were pointed out.

The next step of this research programme would be to simulate the turbulent wake phenomena for flow past a tapered cylinder at higher Reynolds numbers, typically $3\,900 < \mathrm{Re} < 5\,000$, in order to enable comparisons with the experimental study of Hsiao & Chiang (1998). This will be accomplished by means of large-eddy simulations, in which parts of the turbulent fluctuations are accounted for by a sub-grid-scale model.

ACKNOWLEDGEMENTS

This work has received support from The Research Council of Norway (Programme for Supercomputing) through a grant of computing time. The first author was the recipient of a research fellowship offered by The Research Council of Norway under contract no. 121279/410. The authors are grateful to the referees for some helpful suggestions.

REFERENCES

EISENLOHR, H. & ECKELMANN, H. 1989 Vortex splitting and its consequences in the vortex street wake of cylinders at low Reynolds number. *Physics of Fluids* A **1,** 189–192.

GASTER, M. 1969 Vortex shedding from slender cones at low Reynolds numbers. *Journal of Fluid Mechanics* **38,** 565–576.

GASTER, M. 1971 Vortex shedding from circular cylinders at low Reynolds numbers. *Journal of Fluid Mechanics* **46,** 749–756.

GRIFFIN, O. M. 1985 Vortex shedding from bluff bodies in a shear flow: a review. *ASME Journal of Fluids Engineering* **107,** 298–306.

HSIAO, F. B. & CHIANG, C. H. 1998 Experimental study of cellular shedding vortices behind a tapered circular cylinder. *Experimental Thermal and Fluid Science* **17,** 179–188.

JENSSEN, C. B. 1994 Implicit multiblock Euler and Navier–Stokes calculations. *AIAA Journal* **32,** 1808–1814.

JENSSEN, C. B. & WEINERFELT, P. Å. 1995 Coarse grid correction scheme for implicit multiblock Euler calculations. *AIAA Journal* **33,** 1816–1821.

JENSSEN, C. B. & WEINERFELT, P. Å. 1998 Parallel implicit time-accurate Navier–Stokes computations using coarse grid correction. *AIAA Journal* **36,** 946–951.

JESPERSEN, D. C. & LEVIT, C. 1991 Numerical simulation of flow past a tapered cylinder. *AIAA paper* **91–0751**.

MAIR, W. A. & STANSBY, P. K. 1975 Vortex wakes of bluff cylinders in shear flow. *SIAM Journal on Applied Mathematics* **28,** 519–540.

MONKEWITZ, P. A. 2000 Modelling of vortex shedding from cylinders with span-wise non-uniformities. Invited lecture at *IUTAM Symposium on Bluff Body Wakes and Vortex-Induced Vibrations*, Marseille, France, 13–16 June.

MUKHOPADHYAY, A., VENUGOPAL, P. & VANKA, S. P. 1999 Numerical study of vortex shedding from a circular cylinder in linear shear flow. *ASME Journal of Fluids Engineering* **121,** 460–468.

NOACK, B. R., OHLE, F. & ECKELMANN, H. 1991 On cell formation in vortex streets. *Journal of Fluid Mechanics* **227,** 293–308.

PAPANGELOU, A. 1992 Vortex shedding from slender cones at low Reynolds numbers. *Journal of Fluid Mechanics* **242,** 299–321.

PICCIRILLO, P. S. & VAN ATTA, C. W. 1993 An experimental study of vortex shedding behind linearly tapered cylinders at low Reynolds number. *Journal of Fluid Mechanics* **246,** 163–195.

STANSBY, P. K. 1976 The locking-on of vortex shedding due to the cross-stream vibration of circular cylinders in uniform and shear flows. *Journal of Fluid Mechanics* **74,** 641–665.

TRITTON, D. J. 1959 Experiments on the flow past a circular cylinder at low Reynolds numbers. *Journal of Fluid Mechanics* **6,** 547–567.

TRITTON, D. J. 1971 A note on vortex streets behind circular cylinders at low Reynolds numbers. *Journal of Fluid Mechanics* **45,** 203–208.

VALLÈS, B., JENSSEN, C. B. & ANDERSSON, H. I. 2001 Three-dimensional numerical simulation of laminar flow past a tapered circular cylinder. In *Parallel Computational Fluid Dynamics-Trends and Applications*, (eds C. B. Jenssen *et al.,*), pp. 581–588. Amsterdam: Elsevier Science.

WILLIAMSON, C. H. K. 1988 Defining a universal and continuous Strouhal–Reynolds number relationship for the laminar vortex shedding of a circular cylinder. *Physics of Fluids* **31,** 2742–2744.

WILLIAMSON, C. H. K. 1989 Oblique and parallel modes of vortex shedding in the wake of a circular cylinder at low Reynolds numbers. *Journal of Fluid Mechanics* **206,** 579–627.

WILLIAMSON, C. H. K. 1996 Vortex dynamics in the cylinder wake. *Annual Review of Fluid Mechanics* **28**, 477–539.

WILLIAMSON, C. H. K. & BROWN, G. L. 1998 A series in $1/\sqrt{\mathrm{Re}}$ to represent the Strouhal–Reynolds number relationship of the cylinder wake. *Journal of Fluids and Structures* **12,** 1073–1085.

ZDRAVKOVICH, M. M. 1997 *Flow Around Circular Cylinders,* Vol. 1: *Fundamentals.* New York: Oxford University Press.